Appendix A: Line frequencies

Line frequencies were determined by fitting the observed lines with a specific line profile typical of expanding envelopes. The sharp edges of the lines permit us to fit their central frequencies, even when signals are weak, with an accuracy well below 0.5 MHz (Cernicharo et al. 2018). Only when lines are heavily blended is it not possible to accurately derive their frequencies, or even to fit them. Two of the S 1 doublets are heavily blended (N = 29-28 and 37-36). Some doublets (N = 17-16, 27-26, 28-27, and 34-33) show some blending, but the frequencies can still be derived by fixing the linewidths to 29 km s^{-1} (Cernicharo et al. 2000, 2018). The signal-to-noise ratio for the doublets N = 39-38 and 40-39 is low, and therefore we assigned a large uncertainty to their frequencies. We note that due to the increase in linewidth (in MHz) with frequency, the pair of lines of each doublet start to overlap for $N_{up} > 16$. Table A.1 gives the observed and fitted line frequencies for S 1. The series of doublets S 2 are only detected in the 3 mm data. They also show significant blending with other features, as indicated in Figs. 1 and 2. Observed and fitted line frequencies for these doublets are given in Table A.2. The intensity of the observed lines is also provided in the tables.

Appendix B: Possible carriers of the S1 and S2 series

The very close rotational constants of S 1 and S 2 could suggest that they belong to a common molecular carrier. However, the dependence of the line intensity with N is very different. In the case of S 2, low N lines are weak and marginally detected in the Q band, while high N lines are clearly detected in the 3 mm domain; instead, for S 1 the lines are well detected in the Q band and start to vanish at the high end of the 3 mm band. Clearly the two series of doublets arise from two molecular species with different permanent dipole moments. Moreover, the possibility that S 2 is a bending state of S 1 seems very unlikely for the same reasons and because this state will have a $^2\Pi$ vibronic character. In addition, if S 2 were a bending state of S 1 we could expect another series of doublets as the bending introduces an l-doubling as occurs in linear $^1\Sigma$ molecules. The expected value of q, the l-doubling parameter, is a few tens of MHz. Hence, we searched in our data for other series with the same splitting of 4.7 MHz. No obvious candidates were found for a range of 2000 MHz around each observed doublet of S 2.

The difference in line intensities also precludes the possibility that S 1 and S 2 could correspond to the four components of the rotational transitions $N \rightarrow N-1$ of a $^4\Sigma$ electronic state. For such a carrier, the intensities of the four components are proportional to $J(J = N + S)$, hence very similar for the values of N involved in our data. Moreover, this possible carrier needs to have a rather low spin-spin interaction constant in view of the very close frequencies of the four components for each rotational quantum number N.

The rotational constants of S 1 and S 2 are very close to those of well-known molecular species in this source: HC_5N, C_6H, C_5N^-, and C_5N. However, the distortion constants are a factor of 1.4-2 higher for our doublets than for these species. C_6H has several bending modes. The $^2\Sigma^-$ state of the mode ν_{11} of C_6H, which shows a series of doublets with integer harmonic relations, has been characterized in this source (Cernicharo et al. 2008). The corresponding $^2\Sigma^+$ state could be higher in energy and with frequencies very close to those of the $^2\Sigma^-$ state (Cernicharo et al. 2008). The ν_{10} mode also has a relatively low energy, ~200 cm^{-1} (Bacalla et al. 2016). It will also be split into a $^2\Sigma^-$ and a $^2\Sigma^+$ state, in addition to a $^2\Delta$ state with half integer quantum numbers. However, as for any bending mode, we expect to have a rotational constant larger than for the ground state of the molecule. The S 1 and S 2 doublets have rotational constants lower than that of C_6H in its ground state. Hence, these doublets cannot be assigned to vibrationally excited C_6H in its

Table A.1. Observed rotational transitions of S 1 (MgCCCN).

N_u[a]	J_u[a]	N_l[a]	J_l[a]	Obs.Freq.[b]	Unc.[c]	O-C[d]	Int.[e]
12	11.5	11	10.5	33138.673	0.150	0.075	0.169
12	12.5	11	11.5	33143.008	0.150	0.057	
13	12.5	12	11.5	35900.260	0.080	0.030	0.163
13	13.5	12	12.5	35904.683	0.080	0.100	
14	13.5	13	12.5	38661.866	0.150	0.027	0.245
14	14.5	13	13.5	38666.200	0.150	0.008	
15	14.5	14	13.5	41423.336	0.080	−0.086	0.257
15	15.5	14	14.5	41427.711	0.080	−0.064	
16	15.5	15	14.5	44185.057	0.150	0.079	0.259
16	16.5	15	15.5	44189.232	0.150	−0.099	
17	16.5	16	15.5	46946.648	0.150	0.143	0.275
17	17.5	16	16.5	46950.712	0.150	−0.146	
18	17.5	17	16.5	49708.020	0.150	0.020	0.339
18	18.5	17	17.5	49712.338	0.150	−0.015	
26	25.5	25	24.5	71798.763	0.150	0.131	0.329
26	26.5	25	25.5	71802.981	0.150	−0.003	
27	26.5	26	25.5	74559.941	0.300	0.175[f]	0.340
27	27.5	26	26.5	74564.197	0.150	0.078	
28	27.5	27	26.5	77320.562	0.200	−0.290[g]	
28	28.5	27	27.5	77324.925	0.200	−0.290[g]	
29	28.5	28	27.5	[80081.886]	[0.032]	*n.i.*[h]	
29	29.5	28	28.5	80086.523	0.500	0.284[i]	
30	29.5	29	28.5	82842.847	0.150	−0.020	0.255
30	30.5	29	29.5	82847.014	0.150	−0.207	
31	30.5	30	29.5	85603.749	0.150	−0.046	0.210
31	31.5	30	30.5	85608.518	0.150	0.370	
32	31.5	31	30.5	88364.669	0.150	0.004	0.242
32	32.5	31	31.5	88369.040	0.150	0.022	
33	32.5	32	31.5	91125.390	0.150	−0.087	0.279
33	33.5	32	32.5	91129.844	0.150	0.014	
34	33.5	33	32.5	[93886.229]	[0.042]	*n.i.*[j]	0.279
34	34.5	33	33.5	93890.277	0.200	−0.305	
35	34.5	34	33.5	96646.999	0.150	0.080	0.227
35	35.5	34	34.5	96651.440	0.150	0.168	
36	35.5	35	34.5	99407.472	0.200	−0.073	0.166
36	36.5	35	35.5	99411.815	0.200	−0.083	
37	36.5	36	35.5	102168.400	0.500	0.295	
37	37.5	36	36.5	[102172.458]	[0.055]	*n.i.*[k]	
38	37.5	37	36.5	104928.720	0.500	0.122[l]	0.133
38	38.5	37	37.5	104932.450	0.500	−0.501[l]	
39	38.5	38	37.5	107688.500	0.500	−0.522[l]	0.103
39	39.5	38	38.5	107693.827	0.500	0.452[l]	
40	39.5	39	38.5	110449.410	0.500	0.035[l]	0.131
40	40.5	39	39.5	110453.977	0.500	0.249[l]	

Notes. [a] Quantum numbers N and J of the rotational transition. The subindex u means upper level and l lower level. [b] Observed frequency in MHz. Square brackets indicate a calculated frequency. [c] Uncertainty assigned to the measured frequency in MHz. Square brackets indicate a calculated uncertainty from the fit. [d] Observed frequency minus calculated frequency from the fit in MHz. If *n.i.* the line is not included in the fit. [e] Main beam temperature integrated over the LSR velocity, in K km s^{-1}. The uncertainties are below 15%. [f] Line marginally blended with HC_5N. [g] Line blended with narrow U feature. [h] Line fully blended with HC_7N. [i] Line partially blended with HC_7N. [j] Line blended with C_6H in ν_{11} mode. [k] Line fully blended with H_2C_6. [l] Weak feature.

Table A.2. Observed rotational transitions of $S\,2$ (MgC_4H).

N_u[a]	J_u[a]	N_l[a]	J_l[a]	Obs.Freq.[b]	Unc.[c]	O-C[d]	Int.[e]
26	25.5	25	24.5	71830.149	1.000	−0.943[f]	0.155
26	26.5	25	25.5	71835.629	0.500	−0.147	
27	26.5	26	25.5	74593.987	0.300	0.492	0.147
27	27.5	26	26.5	74597.613	0.300	−0.566	
28	27.5	27	26.5	77355.466	0.300	−0.384	
28	28.5	27	27.5	77361.172	0.300	0.638	
29	28.5	28	27.5	80118.288	0.300	0.133	0.154
29	29.5	28	28.5	80122.274	0.500	*n.i.*[g]	
30	29.5	29	28.5	[82880.409]	[0.081]	*n.i.*[h]	
30	30.5	29	29.5	[82885.093]	[0.082]	*n.i.*[h]	
31	30.5	30	29.5	[85642.610]	[0.078]	*n.i.*[i]	
31	31.5	30	30.5	[85647.294]	[0.076]	*n.i.*[i]	
32	31.5	31	30.5	88404.483	0.200	−0.273	0.164
32	32.5	31	31.5	88409.447	0.200	0.007	
33	32.5	32	31.5	[91166.845]	[0.078]	*n.i.*[j]	
33	33.5	32	32.5	[91171.529]	[0.070]	*n.i.*[j]	
34	33.5	33	33.5	93929.043	0.200	0.166	0.136
34	34.5	33	33.5	93933.779	0.200	0.219	
35	34.5	34	33.5	[96690.848]	[0.092]	*n.i.*[k]	
35	35.5	34	34.5	[96695.531]	[0.079]	*n.i.*[k]	
36	35.5	35	34.5	99452.794	0.500	0.037[l]	0.151
36	36.5	35	35.5	99457.396	0.200	−0.044	
37	36.5	36	35.5	[102214.602]	[0.121]	*n.i.*[g]	
37	37.5	36	36.5	[102219.286]	[0.105]	*n.i.*[g]	
38	37.5	37	36.5	[104976.382]	[0.140]	*n.i.*[m]	0.105
38	38.5	37	37.5	104981.775	1.000	0.709[m]	
39	38.5	38	37.5	107738.266	0.500	0.171	0.082
39	39.5	38	38.5	107741.955	0.500	−0.824	
40	39.5	39	38.5	[110499.739]	[0.186]	*n.i.*[h]	0.074
40	40.5	39	39.5	[110504.422]	[0.169]	*n.i.*[h]	

Notes. [(a)] Quantum numbers N and J of the rotational transition. The subindex u means upper level and l lower level. [(b)] Same as in Table A.1 [(c)] Same as in Table A.1 [(d)] Observed frequency minus calculated frequency from the fit in MHz. If *n.i.* the line is not included in the fit. [(e)] Main beam temperature integrated over the LSR velocity, in K km s^{-1}. The uncertainties are below 30%. [(f)] Line contaminated with KCN. [(g)] Line contaminated with a U-line. [(h)] Line contaminated with HC_4N. [(i)] Line contaminated with C_4H. [(j)] Line contaminated with NaCl. [(k)] Line contaminated with several features. [(l)] Line contaminated with SiH_3CN. [(m)] Line contaminated with ^{13}CCCN.

ν_{10} mode. Moreover, $S\,1$ and $S\,2$ cannot be assigned to the ν_{11} modes of ^{13}C isotopically substituted C_6H as the $^{12}C/^{13}C$ abundance ratio in this source is ∼42 (Cernicharo et al. 1991), and the observed $S\,1$ and $S\,2$ intensities are similar to those of the lines of the ^{13}C isotopologues of C_6H in their ground vibrational state. In addition, six series of doublets, with identical intensity and line separation, could be expected from the ν_{11} vibrational state of the ^{13}C isotopologues of C_6H. The same applies to C_5N, which has a rotational constant larger than C_6H.

The anion HC_5N has been calculated to have a ^2A ground electronic state with $(B + C)/2$ ∼1377 MHz (Jerosimić et al. 2019). The calculation method is very similar to the one used in this work, RHF-CCSD(T)-F12/cc-pVTZ-F12. HC_5N^- would only be compatible with the $S\,1$ or $S\,2$ doublets if we were observing the K_a=0 transitions of HC_5N^-. In this case the effective distortion constant for this asymmetric species would be larger than those obtained for the $S\,1$ and $S\,2$ doublets. We calculated the theoretical value for D_N because it was not reported in the Jerosimić et al. (2019) work at the CCSD(T)/cc-pVTZ level of theory, and we found D_N = 0.28 kHz, almost 4-5 times higher than those of $S\,1$ and $S\,2$. This value is totally incompatible with our experimental values of D for $S\,1$ and $S\,2$. Hence, HC_5N^- cannot be considered as a candidate. In addition, we calculated the spin-rotation constants of HC_5N^-, which are 1203.4, −0.2, and −2.5 MHz for ϵ_{aa}, ϵ_{bb}, and ϵ_{cc}, respectively. They are also different from our experimental value of γ. ClCCCN has a rotational constant of 1382 MHz (Bjorvatten 1974), which is very close to those of $S\,1$ and $S\,2$, although this species has a $^1\Sigma$ ground electronic state. ClC_4 has a $^2\Sigma$ ground electronic state. However, its rotational constant is 1455.6 MHz (Sumiyoshi et al. 2005). SiC_4H (McCarthy et al. 2001) and SiC_3N (Umeki et al. 2014) have a rotational constant of 1415.7 and 1414.7 MHz, respectively, and they have a $^2\Pi$ electronic state.

Petrie (1999) suggested that the species $M-C_3N$ could be abundant in IRC +10216. Two of these species, AlC_3N and NaC_3N, have been observed in the laboratory by Cabezas et al. (2019). They have $^1\Sigma$ ground electronic states and rotational constants close to those of $S\,1$ and $S\,2$ (1340.8 and 1321.1 MHz, respectively). They have been searched for in IRC +10216 without success. Petrie et al. (2003) performed quantum chemical calculations and provided estimations for the rotational constants of MgC_3N and MgC_4H. Both molecules have a $^2\Sigma$ ground electronic state and the calculated rotational constants are very close to those of $S\,1$ and $S\,2$.

Table C.1. Comparison of experimental and theoretical values for the spectroscopic parameters of MgCCH.

MgCCH	Exp.[a]	CCSD(T)-F12[b]	CCSD(T)[c]
B /MHz	4965.335(4)	4947.373[0.4]	4864.358[2.0]
D /kHz	2.232(2)	1.886[15.5][d]	1.933[13.4]
γ/MHz	16.49(4)	15.72[4.7][e]	15.02[8.9][f]

Notes. Numbers in parentheses are 1 σ uncertainties in units of the last digits. Numbers in square brackets are the percentage of relative error calculated as (experimental−theoretical)/experimental. [(a)] Brewster et al. (1999). [(b)] Calculated at the CCSD(T)-F12/cc-pCVTZ-F12 level of theory. [(c)] Calculated at the CCSD(T)/aug-cc-pVTZ level of theory. [(d)] Calculated at the CCSD(T)/cc-pVTZ level of theory. [(e)] Calculated at the MP2/cc-pVTZ level of theory. [(f)] Calculated at the MP2/aug-cc-pVTZ level of theory.

Appendix C: Quantum chemical calculations of MgC_3N and MgC_4H

MgC_3N and MgC_4H have already been investigated by quantum chemical calculations at diverse levels of theory, and some theoretical works are available in the literature (Petrie et al. 2003; Ding et al. 2008; Gou et al. 2009; Forthomme et al. 2010; Cabezas et al. 2019). However, in an attempt to obtain the most precise geometries and spectroscopic molecular parameters for the species MgC_3N and MgC_4H, we performed high-level ab initio calculations using very accurate methods and basis sets.

Further evidence in support of the assignment of MgC_3N to $S\,1$ and MgC_4H to $S\,2$ is related to the constants D and γ. The predicted values, with the geometries optimized either at the CCSD(T)-F12/cc-pCVTZ-F12 or CCSD(T)/aug-cc-pVTZ level, are in very good agreement with those derived from the observations. In addition, a similar comparison of the MgC_3N/MgC_4H constant ratios can be made with the data of Table C.2 and the agreement is almost perfect for both D and γ.

All structure optimization calculations reported in this work were performed using both the spin-restricted open-shell coupled cluster with single, double, and perturbative triple excitations (CCSD(T)) with and without an explicitly correlated (F12) approximation (Adler et al. 2007; Knizia et al. 2009).

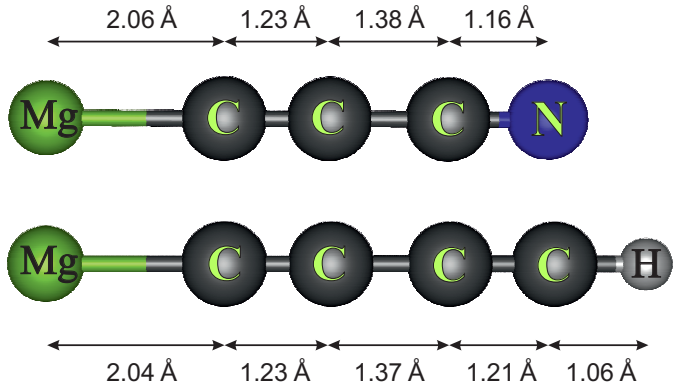

Fig. C.1. MgCCCN (top) and MgCCCCH (bottom) optimized structures at the CCSD(T)-F12/cc-pCVTZ-F12 level of theory.

Table C.2. Comparison of experimental and theoretical values for the spectroscopic parameters of MgCCCN and MgCCCCH.

MgCCCN	Exp.[a]	CCSD(T)-F12[b]	CCSD(T)[c]
B /MHz	1380.888(1)	1376.4990[0.3]	1357.6663[1.7]
D /kHz	0.0760(5)	0.0644[15.3][d]	0.0649[14.6]
γ/MHz	4.35(4)	4.09[5.9][e]	3.93[9.7][f]
μ /D		6.38	6.39
MgCCCCH	Exp.[a]	CCSD(T)-F12[b]	CCSD(T)[c]
B /MHz	1381.512(4)	1377.3833[0.3]	1358.4109[1.7]
D /kHz	0.074(2)	0.0605[18.2][d]	0.0614[17.0]
γ/MHz	4.7(1)	4.43[5.7][e]	4.24[9.8][f]
μ /D		2.12	2.16
Ratio[g]	Exp.[a]	CCSD(T)-F12[b]	CCSD(T)[c]
B	0.9996	0.9994	0.9995
D	1.0270	1.0645[d]	1.0576[d]
γ	0.9255	0.9238[e]	0.9266[e]

Notes. Numbers in parentheses are 1 σ uncertainties in units of the last digits. Numbers in square brackets are the percentage of relative error calculated as (experimental−theoretical)/experimental. [(a)] This work. [(b)] Calculated at the CCSD(T)-F12/cc-pCVTZ-F12 level of theory. [(c)] Quantum chemical calculation results at the CCSD(T)/aug-cc-pVTZ level of theory. [(d)] Calculated at the CCSD(T)/cc-pVTZ level of theory. [(e)] Calculated at the MP2/cc-pVTZ level of theory. [(f)] Calculated at the MP2/aug-cc-pVTZ level of theory. [(g)] Ratio MgCCCN/MgCCCCH of the spectroscopic constant.

The Dunning's augmented correlation consistent polarized valence triple-ζ (aug-cc-pVTZ) basis set, where only valence electrons are correlated, was used with the CCSD(T) method. On the other hand, with the calculations at the CCSD(T)-F12 level, the Dunning's correlation consistent basis sets with polarized core-valence correlation triple-ζ for explicitly correlated calculations (cc-pCVTZ-F12; Hill et al. 2010a,b) was used. In this latter case, all electrons (valence and core) were correlated. Using both levels of theory, the equilibrium molecular geometries, rotational constants, and dipole moments μ were calculated for MgC_3N and MgC_4H in their ground electronic states using the Molpro 2018.1 ab initio program package (Werner et al. 2018).

An important molecular parameter needed to precisely simulate the rotational spectra of MgC_3N and MgC_4H at the observed frequency regions is the centrifugal distortion constant (D). This constant was obtained by subsequent harmonic vibrational calculations at the CCSD(T)/cc-pVTZ and CCSD(T)/aug-cc-pVTZ levels of theory. Since MgC_3N and MgC_4H are open-shell species, the spin-rotation constant γ is another parameter to take into account to adequately estimate the transition rotational frequencies. It was calculated at the MP2/cc-pVTZ and MP2/aug-cc-pVTZ levels of theory using the optimized structures at the CCSD(T)-F12/cc-pCVTZ-F12 and CCSD(T)/aug-cc-pVTZ levels of theory, respectively. We used different calculations methods for D and γ because they cannot be calculated with explicitly correlated methods, and thus the Gaussian 16 program package was used (Frisch et al. 2016).

Table C.3. Harmonic vibrational frequencies of MgCCCN calculated at the CCSD(T)/cc-pVTZ level.

Mode	Symmetry	Frequency (cm^{-1})	IR intensity[a] (km/mole)
1	π	76	0.16
2	π	257	6.43
3	σ	391	82.35
4	π	508	3.16
5	σ	933	75.71
6	σ	2083	15.86
7	σ	2299	3.54

Notes. [(a)] I ntensities calculated at the MP2/aug-cc-pVTZ level of theory.

Although MgC_3N and MgC_4H present different structural isomers, i.e. linear, cyclic, or T-shaped (Petrie et al. 2003; Cabezas et al. 2019), we only considered the lowest energy isomers with $^2\Sigma^+$ linear structures: MgCCCN and MgCCCCH. The geometry optimizations were done at both the CCSD(T)/aug-cc-pVTZ and CCSD(T)-F12/cc-pCVTZ-F12 methods, because the data obtained with the latter method was the most accurate. It has been demonstrated (Adler et al. 2007; Knizia et al. 2009) that the F12 correction strongly improves the basis set convergence for a wide variety of applications, including reaction energies of both open- and closed-shell reactions, atomization energies, electron affinities, equilibrium geometries, or harmonic vibrational frequencies. In addition, correlation consistent basis sets such as cc-pCVTZ-F12 have been optimized for accurately describing core-core and core-valence correlation effects with explicitly correlated F12 methods.

The reliability of the two methods of calculation was tested in the case of MgCCH. The CCSD(T)/aug-cc-pVTZ and CCSD(T)-F12/cc-pCVTZ-F12 predicted rotational constants for MgCCH are 4864.36 and 4947.37 MHz, respectively, while the experimental value for MgCCH is 4965.3346 ± 0.0038 MHz (Brewster et al. 1999). The relative percentage deviation in the calculation, $(((B_{exp} - B_{th})/B_{exp}) \times 100)$, is 2.03 % for CCSD(T)/aug-cc-pVTZ, but only 0.36 % when CCSD(T)-F12/cc-pCVTZ-F12 is used. Therefore, it seems that the latter level of calculation is reliable for predictive purposes in magnesium-bearing compounds.

The constants D and γ were calculated for MgCCH and the results, shown in Table C.1, point to discrepancies that are substantially larger than for the rotational constant B. However, the values of D and γ calculated at the CCSD(T)/cc-pVTZ and MP2/cc-pVTZ levels are accurate enough, considering that the precise estimation of these values by ab initio calculations is complicated.

The results of our calculations for MgCCCN and MgCCCCH are summarized in Table C.2 and the optimized geometries are shown in Fig. C.1. Tables C.3, C.4, and C.5 show harmonic vibrational frequencies and infrared band intensities of MgCCCN, MgCCCCH, and MgCCH, respectively, calcu-

Table C.4. Harmonic vibrational frequencies of MgCCCCH calculated at the CCSD(T)/cc-pVTZ level.

Mode	Symmetry	Frequency (cm^{-1})	IR intensity[a] (km/mole)
1	π	71	6.94
2	π	253	0.10
3	σ	403	85.13
4	π	502	0.56
5	π	607	40.38
6	σ	949	62.00
7	σ	2033	53.86
8	σ	2213	2.72
9	σ	3460	95.99

Notes. [(a)] I ntensities calculated at the MP2/aug-cc-pVTZ level of theory.

Table C.5. Harmonic vibrational frequencies of MgCCH calculated at the CCSD(T)/cc-pVTZ level.

Mode	Symmetry	Frequency (cm^{-1})	IR intensity[a] (km/mole)
1	π	156	11.82
2	σ	492	98.86
3	π	659	38.83
4	σ	2055	20.69
5	σ	3428	24.96

Notes. [(a)] I ntensities calculated at the MP2/aug-cc-pVTZ level of theory.

lated at the CCSD(T)/cc-pVTZ level of theory. As in the case of MgCCH, the errors between the experimental and calculated rotational constants at the CCSD(T)-F12/cc-pCVTZ-F12 level of theory are very small, 0.3 % in both cases when MgCCCN and MgCCCCH are assigned to $S1$ and $S2$, respectively. In the same way, the errors are larger when the CCSD(T)/aug-cc-pVTZ level is used, 1.7 % for both MgCCCN and MgCCCCH, while for MgCCH it is 2.0 %. This indicates that, independently of the level of the calculation, the assignments of MgCCCN to $S1$ and MgCCCCH to $S2$ provides discrepancies of the same order, which supports the identification of these species. The same conclusion can be reached if we compare the ratios between the experimental rotational constants of MgCCCN ($S1$) and MgCCCCH ($S2$), $B_{exp}(MgC_3N)/B_{exp}(MgC_4H)$, with those obtained from the theoretical calculations, $B_{th}(MgC_3N)/B_{th}(MgC_4H)$. The ratio for the experimental rotational constants is 0.9996, while those for the CCSD(T)-F12/cc-pCVTZ-F12 and CCSD(T)/aug-cc-pVTZ levels, respectively, are 0.9994 and 0.9995, in excellent agreement with the experimental value.

Previous quantum chemical calculations for MgCCCN have been reported by Petrie et al. (2003) and Cabezas et al. (2019). In their work, Petrie et al. (2003) used the B3LYP, MP3, CCSD, and CCSD(T) methods in conjunction with some basis sets. The corrected value for the rotational constant of MgCCCN using CCSD(T)/cc-pVDZ is 1383.3 MHz, which is not far from the experimental value. Cabezas et al. (2019) calculated the rotational constant, with the estimated vibration-rotation interaction constants by second-order perturbation theory at the MP2/aug-cc-pVTZ level, and found an overestimated value of 1391.3 MHz, 0.75% higher than the experimental value.

Ding et al. (2008) and Gou et al. (2009) reported theoretical values for the rotational constant of MgCCCCH using B3LYP, RCCSD(T) and CASSCF methods. The values found by Ding et al. (2008) are 1382.5 MHz when using the B3LYP/aug-cc-pVTZ and 1351.4 MHz at the RCCSD(T)/aug-cc-pVTZ level of theory. The latter value is a bit lower than that reported in this work using the same level of theory, 1358.41 MHz. On the other hand, Gou et al. (2009) used more modest levels of theory and obtained B values of 1373.3 and 1360.8 MHz at the B3LYP/6-31G* and CASSCF/6-31G* levels.

Appendix D: The role of infrared pumping of polyatomic molecules

Infrared pumping of polyatomic molecules could strongly affect the population of the rotational levels of the ground vibrational state of the considered species. The pumping is produced by absorption of photons from a level J_{low} to a level of any of the ro-vibrational modes with total quantum number $J_{up} = J_{low} \pm 1$ (ΔJ=0 transitions are also allowed if bending is considered), followed by fast decay to levels of the ground state with $J = J_{up} \pm 1$. These up and down radiative cascades can populate levels of high J that will normally be weakly pumped by collisions. Agúndez & Cernicharo (2006) showed that IR pumping in molecules like water can produce errors as large as a factor of ten in the determination of the column density. Similar effects apply to triatomic species such as CCH and HNC (Cernicharo et al. 2014).

The role of infrared pumping of the simple polyatomic molecule HNC has been analysed by Cernicharo et al. (2014). Each mode affects the pumping of the ground state in a different way as it depends on the vibrational intensity, the size of the IR emitting region, and the temperature of the dust. Infrared pumping through stretching modes (frequencies above 1000 cm^{-1}) is produced by photons arising from a warm and very small region (e.g. the dust formation zone for IRC+10216, which has a diameter <1″). However, the pumping through the bending states depends strongly on the frequency of the vibrational mode. The size of the emitting region for frequencies below 100 cm^{-1} can be much larger than those producing infrared pumping through the stretching modes.

In addition to the fundamental modes we have to consider all the combination modes involving two bendings, and one bending plus one stretching that are strongly radiatively connected to the ground. The number of infrared cascades increases considerably with the number of atoms. Agúndez et al. (2017) have performed some simple models for C_nH radicals and cyanopolyynes species ($HC_{2n+1}N$) showing that infrared pumping can modify the spatial distribution of each species and has a important effect on the observed intensities. MgC_3N has seven vibrational modes (see Table C.3), MgC_4H has nine (see Table C.4), while MgCCH has only only five (see Table C.5). Hence, while MgC_3N and MgC_4H could have similar infrared pumping effects, they could be very different to those of MgCCH. A detailed modelling is really complex and is beyond the scope of the present work. The derived column densities, and the MgC_4H/MgCCH abundance ratio, should be considered with caution.

Appendix E: Confirmation of MgCCH in space

MgCCH was tentatively detected by Agúndez et al. (2014) on the basis of the two doublets N = 9-8 and 10-9. Since these observations, additional data of IRC +10216 have been collected at 3 and 2 mm with the IRAM 30m telescope (Cernicharo et al. 2018,

2019). The lines presented by Agúndez et al. (2014) at 3 mm are very weak (T_A^* ~2 mK) and the detection of additional doublets was only possible when the sensitivity of the data reached a level below 1 mK.

Figure E.1 shows the data for all doublets of MgCCH up to N = 17-16. The signal-to-noise ratio of the 3 mm data has improved and the two doublets N = 9-8 and 10-9 now appear at a high confidence level. Additional doublets without blending from other features are N = 15-14 and 16-15. For the N = 11-10 doublet, the $J = N - 1/2$ component is fully blended with a component of N = 1-0 transition of ^{13}CN. However, the $J = N + 1/2$ component is clearly detected. For the N = 13-12 doublet, although the bulk of the emission is blended with NaCN, the left side of $J = N - 1/2$ component is visible and the same happens for the right side of the $J = N + 1/2$ component. In the case of the N = 14-13 doublet only the $J = N + 1/2$ component appears clearly. Although the other component is marginally present, the sensitivity of the data and probable baseline problems at these noise levels prevent its confident detection. Finally, the N = 17-16 has a poor signal-to-noise ratio and the $J = N - 1/2$ component is partially blended with H_2S. However, the $J = N+1/2$ component is detected with an intensity similar to that of the other doublets.

Hence, on the basis of four doublets and five additional features agreeing with the $J = N - 1/2$ or $J = N + 1/2$ components of other doublets, we conclude that MgCCH can be considered as detected in IRC +10216. We derive a column density for MgCCH identical to that derived by Agúndez et al. (2014), i.e. N(MgCCH) ~2×10^{12} cm^{-2}.

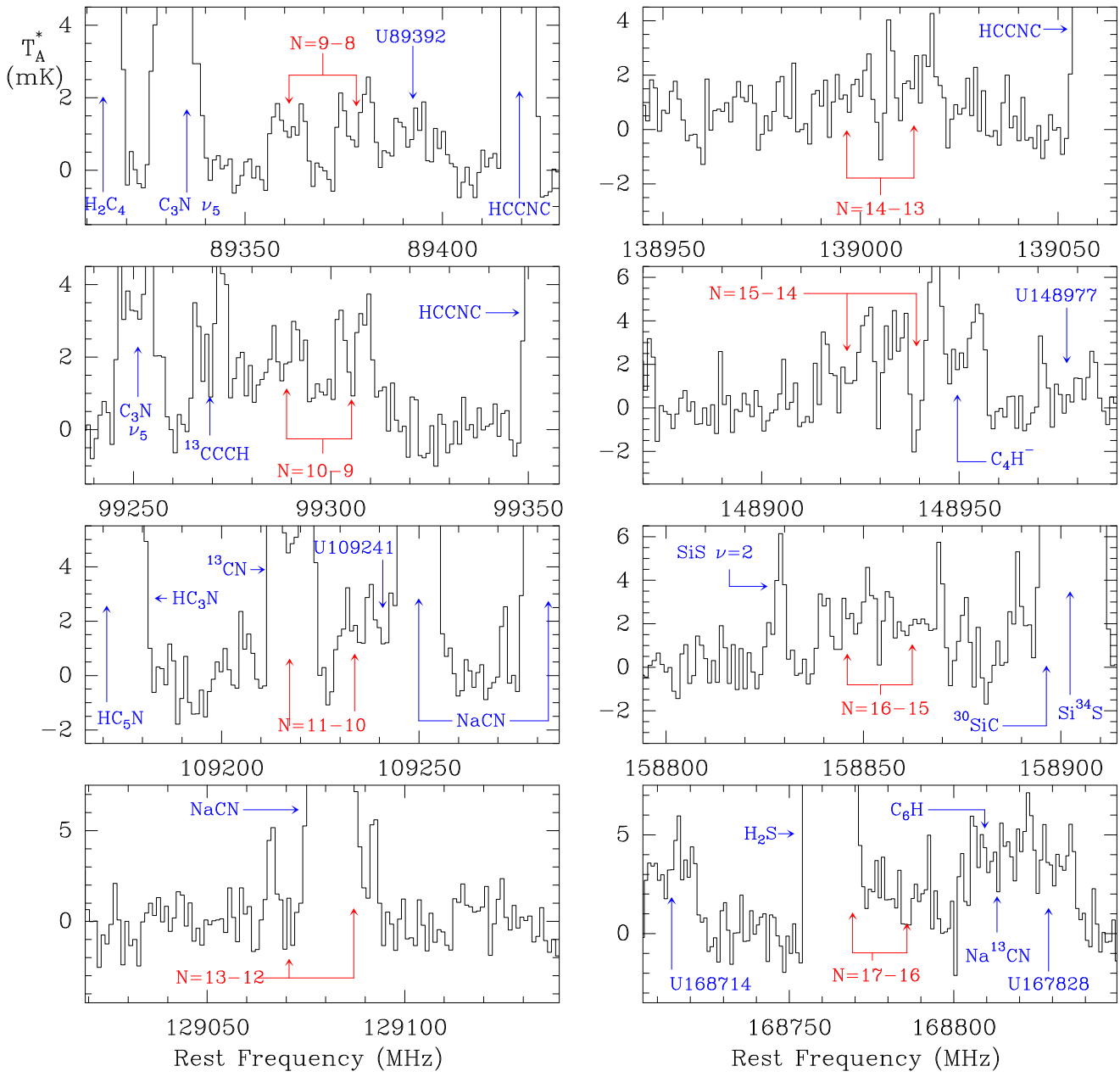

Fig. E.1. Observed doublets of MgCCH towards IRC+10216 (black histogram). The vertical scale is the antenna temperature in mK, and the horizontal scale is the frequency in MHz. Labels for the lines of MgCCH are plotted in red in each panel. Unidentified (U) lines are indicated in blue.